Eur. J. Mech. B/Fluids, **18**, (1), 103-119, 1999

Monte Carlo simulation of the heat flow in a dense hard sphere gas

A. FREZZOTTI

ABSTRACT. – The one-dimensional steady heat flow in a dense hard sphere gas is studied solving the Enskog equation numerically by a recently proposed DSMC-like particle scheme. The accuracy of the solutions is assessed through a comparison with solutions obtained from a semi-regular method which combines finite difference discretization with Monte Carlo quadrature techniques. It is shown that excellent agreement is found between the two numerical methods. The solutions obtained from the Enskog equation have also been found in good agreement with the results of molecular dynamics simulations. © Elsevier, Paris.

Keywords. – Enskog equation, Monte Carlo, heat flow, molecular dynamics.

1. Introduction

In this paper steady one-dimensional heat flow is studied in a hard sphere gas in which the mean free path and the molecular diameter have the same order of magnitude. The gas molecules are confined in the gap between two infinite parallel plates kept at different temperatures. The temperature is uniform on the plate surfaces and constant in time. Since the plates can be only a few mean free paths (or molecular diameters) apart a kinetic theory approach should be taken in the study of this problem. Accordingly, it is assumed that the fluid motion is governed by the following kinetic equation:

$$\frac{\partial F}{\partial t} + \boldsymbol{\xi} \circ \nabla F = J_E(F,F) \tag{1}$$

$$\begin{aligned} J_E(F,F) = a^2 \int \Bigg\{ & Y\left[n\left(\mathbf{x} + \frac{a}{2}\hat{\mathbf{k}}, t\right)\right] F(\mathbf{x} + a\hat{\mathbf{k}}, \boldsymbol{\xi}_1^*, t) F(\mathbf{x}, \boldsymbol{\xi}^*, t) \\ & - Y\left[n\left(\mathbf{x} - \frac{a}{2}\hat{\mathbf{k}}, t\right)\right] F(\mathbf{x} - a\hat{\mathbf{k}}, \boldsymbol{\xi}_1, t) F(\mathbf{x}, \boldsymbol{\xi}, t) \Bigg\} H(\boldsymbol{\xi}_r \circ \hat{\mathbf{k}})(\boldsymbol{\xi}_r \circ \hat{\mathbf{k}}) d\boldsymbol{\xi}_1 d^2\hat{\mathbf{k}} \end{aligned} \tag{2}$$

which was proposed by Enskog (1922) as an extension of the Boltzmann equation to dense fluids.

In Eqs. (1-2) $F(\mathbf{x}, \boldsymbol{\xi}, t)$ is the one-particle distribution function of the molecular velocities $\boldsymbol{\xi}$, $\boldsymbol{\xi}_r = \boldsymbol{\xi}_1 - \boldsymbol{\xi}$ is the relative velocity of two colliding molecules, whereas $\hat{\mathbf{k}}$ is a unit vector which specifies their relative position at the time of impact. The factor $Y(n)$ is a given function of the density, which plays the role of a velocity-independent pair correlation function (Resibois and DeLeener, 1977) and, in the simplest formulation of Enskog equation (van Beijeren and Ernst, 1973), it is set equal to the value of the uniform equilibrium pair correlation function at the contact position (Resibois and DeLeener, 1977).

Dipartimento di Matematica del Politecnico di Milano, Piazza Leonardo da Vinci 32, 20133 Milano, Italy.

0997-7546/99/01/© Elsevier, Paris

It is clear that the Enskog equation should be regarded as a phenomelogical equation; nevertheless recent investigations (Frezzotti, 1998; Frezzotti 1997a) have shown that shock wave profiles obtained from the numerical solution of Eq. (1) exhibit very good agreement with molecular dynamics (MD) simulations, even at relatively high densities. On the other hand, in the study of the density profile in a hard sphere gas in equilibrium near a reflecting wall (Frezzotti, 1997a), evidence has been found that the Enskog theory calculations start deviating from the correct result above a certain density threshold.

Following the indications of Frezzotti (1997a), this paper aims at presenting a more systematic analysis of the limitations of Enskog equation, whose solutions are compared to MD results. The heat conduction problem considered here is particularly well suited for such an investigation because of its simple geometry and the possibility of obtaining large density variations by coupling the effects of the temperature gradient to the presence of solid boundaries. Moreover, the problem lends itself to an easy mathematical treatment in the continuum limit, thus providing a further useful test for the numerical computations.

2. Formulation of the problem and basic equations

As mentioned in the previous section, we study the problem of the heat conduction in a gas whose molecules behave as perfectly elastic spheres of diameter a. The centres of the molecules are confined in the region $\mathbb{D} = \{(x, y, z) \in \mathbb{R}^3 : 0 \leq x \leq L\}$ by two infinite planar walls normal to the x axis and located at $x_1 = -\frac{a}{2}$ and $x_2 = L + \frac{a}{2}$, respectively. The wall located at x_i is kept at the uniform and constant temperature T_i and, without loss of generality, it will be assumed that $T_1 \leq T_2$. The boundary conditions are compatible with the existence of a steady, one-dimensional solution of Eq. (1); hence a solution $F(x, \boldsymbol{\xi})$ of the equation:

$$\xi_x \frac{\partial F}{\partial x} = J_E(F, F) \tag{3}$$

is sought in the interval $0 \leqq x \leqq L$ with the following boundary conditions:

$$F(0, \boldsymbol{\xi}) = \frac{n_1}{(2\pi RT_1)^{3/2}} \exp\left[-\frac{\boldsymbol{\xi}^2}{2RT_1}\right] \qquad \xi_x > 0 \tag{4}$$

$$F(L, \boldsymbol{\xi}) = \frac{n_2}{(2\pi RT_2)^{3/2}} \exp\left[-\frac{\boldsymbol{\xi}^2}{2RT_2}\right] \qquad \xi_x < 0. \tag{5}$$

According to Eqs. (4, 5), it is assumed that a molecule hitting a wall completely "forgets" its past history and it is immediately reemitted with a random velocity obtained by sampling the outgoing flux distributions $\xi_x F(0, \boldsymbol{\xi})$ and $\xi_x F(L, \boldsymbol{\xi})$. The parameters n_i are determined by the condition of zero net mass flux at the walls:

$$n_1 \sqrt{\frac{RT_1}{2\pi}} = -\int_{\xi_x < 0} \xi_x F(0, \boldsymbol{\xi}) d\boldsymbol{\xi} \tag{6}$$

$$n_2 \sqrt{\frac{RT_2}{2\pi}} = -\int_{\xi_x > 0} \xi_x F(L, \boldsymbol{\xi}) d\boldsymbol{\xi}. \tag{7}$$

An approximate value for the pair correlation function at contact, $Y(n)$, can be obtained from the equation of state of the gas using the following relationship (Resibois and DeLeener, 1977):

$$Y(n) = \frac{1}{nb}\left(\frac{p}{nkT} - 1\right), \tag{8}$$

p being the pressure and $b = \frac{2\pi a^3}{3}$. The equation of state of the hard sphere fluid cannot be given in closed form, but various approximate expressions have been proposed (Balescu, 1975). In this work the approximation by Carnahan and Starling (1969) has been used:

$$\frac{p}{nkT} = \frac{1 + \eta + \eta^2 - \eta^3}{(1-\eta)^3} \tag{9}$$

$$\eta = \frac{\pi a^3 n}{6}. \tag{10}$$

Combining the above equations yields:

$$Y(n) = \frac{1}{2}\frac{2-\eta}{(1-\eta)^3}. \tag{11}$$

It is worth noticing that the singularity at $\eta = 1$ has no physical meaning, being a mere artifact of the approximations used to derive Eq. (9) which retains its accuracy up to $\eta \approx 0.47$, where the hard sphere fluid undergoes a liquid to solid phase transition.

Once the solution of Eq. (3) has been obtained, some important macroscopic quantities can be obtained as moments of F:

$$n(x) = \int F(x, \boldsymbol{\xi}) d\boldsymbol{\xi} \quad \text{number density} \tag{12}$$

$$\mathbf{u}(x) = \frac{1}{n(x)} \int \boldsymbol{\xi} F(x, \boldsymbol{\xi}) d\boldsymbol{\xi} \quad \text{mean velocity} \tag{13}$$

$$T(x) = \frac{1}{3n(x)R} \int (\boldsymbol{\xi} - \mathbf{u})^2 F(x, \boldsymbol{\xi}) d\boldsymbol{\xi} \quad \text{temperature.} \tag{14}$$

However a few other significant quantities also involve moments of the collision integral. When Eq. (1) is multiplied by the collision invariants $\phi_1(\boldsymbol{\xi}) = 1, \phi_2(\boldsymbol{\xi}) = m\xi_x$, $\phi_3(\boldsymbol{\xi}) = m\frac{\xi^2}{2}$ and the integration over $\boldsymbol{\xi}$ is performed, the following balance equations are obtained:

$$\frac{\partial}{\partial x} \int \xi_x \phi_i(\boldsymbol{\xi}) F(x, \boldsymbol{\xi}) d\boldsymbol{\xi} = \int J_E(F, F) \phi_i(\boldsymbol{\xi}) d\boldsymbol{\xi} \quad i = 1, 2, 3. \tag{15}$$

The collision integral conserves mass locally, therefore the integral for ϕ_1 at the r.h.s. of Eq. (15) vanishes and the first of the three above equations will just express the mass conservation in the following simple form:

$$n(x) u_x(x) = const. \tag{16}$$

$u_x(x)$ being the x component of $\mathbf{u}$. The walls are not permeable, hence the mass flux has to vanish at the boundaries and Eq. (16) gives $u_x(x) \equiv 0$. The local collisional rates of change of momentum (ϕ_2) and energy

(ϕ_3) do not vanish for the Enskog equation, but it is possible to put them in divergence form, since the following general result holds (Cercignani and Lampis, 1988):

$$m \int \boldsymbol{\xi} J_E(F,F) d\boldsymbol{\xi} = -\nabla \circ \boldsymbol{P}^{\rm pot}(\mathbf{x},t) \tag{17}$$

$$m \int \frac{\boldsymbol{\xi}^2}{2} J_E(F,F) d\boldsymbol{\xi} = -\nabla \circ \boldsymbol{Q}^{\rm pot}(\mathbf{x},t). \tag{18}$$

The potential part of the stress tensor $\boldsymbol{P}^{\rm pot}(\mathbf{x},t)$ and heat flux vector $\boldsymbol{Q}^{\rm pot}(\mathbf{x},t)$ are defined as:

$$\boldsymbol{P}^{\rm pot}(\mathbf{x},t) = -m\frac{a^2}{2} \int d\boldsymbol{\xi}_1\, d\boldsymbol{\xi}_2\, d^2\hat{\mathbf{k}} \int_0^a d\alpha (\boldsymbol{\xi}_1^* - \boldsymbol{\xi}_1)\hat{\mathbf{k}} Y\left[n\left(\mathbf{x} + \alpha\hat{\mathbf{k}} - \frac{a}{2}\hat{\mathbf{k}}\right)\right] \tag{19}$$
$$F(\mathbf{x} + \alpha\hat{\mathbf{k}} - a\hat{\mathbf{k}}, \boldsymbol{\xi}_1, t) F(\mathbf{x} + \alpha\hat{\mathbf{k}}, \boldsymbol{\xi}_2, t)(\boldsymbol{\xi}_r \circ \hat{\mathbf{k}}) H(\boldsymbol{\xi}_r \circ \hat{\mathbf{k}})$$

$$\boldsymbol{Q}^{\rm pot}(\mathbf{x},t) = -m\frac{a^2}{4} \int d\boldsymbol{\xi}_1\, d\boldsymbol{\xi}_2\, d^2\hat{\mathbf{k}} \int_0^a d\alpha (\boldsymbol{\xi}_1^{*2} - \boldsymbol{\xi}_1^2)\hat{\mathbf{k}} Y\left[n\left(\mathbf{x} + \alpha\hat{\mathbf{k}} - \frac{a}{2}\hat{\mathbf{k}}\right)\right] \tag{20}$$
$$F(\mathbf{x} + \alpha\hat{\mathbf{k}} - a\hat{\mathbf{k}}, \boldsymbol{\xi}_1, t) F(\mathbf{x} + \alpha\hat{\mathbf{k}}, \boldsymbol{\xi}_2, t)(\boldsymbol{\xi}_r \circ \hat{\mathbf{k}}) H(\boldsymbol{\xi}_r \circ \hat{\mathbf{k}}).$$

Using the above expressions, it is possible to transform the second and third equation in (15) as follows:

$$P_{xx}(x) = P_{xx}^{\rm kin}(x) + P_{xx}^{\rm pot}(x) = const. \tag{21}$$

$$Q_x(x) = Q_x^{\rm kin}(x) + Q_x^{\rm pot}(x) = const. \tag{22}$$

In Eqs. (21, 22) P_{xx} is the xx component of the total stress tensor $\boldsymbol{P} = \boldsymbol{P}^{\rm kin} + \boldsymbol{P}^{\rm pot}$, whereas Q_x is the x component of the total heat flux vector $\boldsymbol{Q} = \boldsymbol{Q}^{\rm kin} + \boldsymbol{Q}^{\rm pot}$. The kinetic stress tensor and heat flux are defined as:

$$\boldsymbol{P}^{\rm kin}(\mathbf{x},t) = m \int \boldsymbol{cc} F(\mathbf{x},\boldsymbol{\xi},t)\, d\boldsymbol{\xi} \tag{23}$$

$$\boldsymbol{Q}^{\rm kin}(\mathbf{x},t) = \frac{m}{2} \int \boldsymbol{c}\boldsymbol{c}^2 F(\mathbf{x},\boldsymbol{\xi},t) d\boldsymbol{\xi} \tag{24}$$

$\boldsymbol{c} = \boldsymbol{\xi} - \mathbf{u}$ being the peculiar velocity.

3. Description of the numerical results

3.1. Sketch of numerical method

Approximate solutions of the problem outlined in the previous section have been obtained by the Monte Carlo simulation method described in (Frezzotti, 1997b). The algorithm is based on a particle scheme in which the

distribution function $F(\mathbf{x}, \boldsymbol{\xi}, t)$ is represented by N_p particles and takes the following form:

$$F(\mathbf{x}, \boldsymbol{\xi}, t) = \sum_{i=1}^{N_p} \delta(\mathbf{x} - \mathbf{x}_i(t))\delta(\boldsymbol{\xi} - \boldsymbol{\xi}_i(t)) \tag{25}$$

$\mathbf{x}_i(t)$ and $\boldsymbol{\xi}_i(t)$ being the position and the velocity of particle i at time t, respectively. Time is discretized and the particle positions and velocities are advanced from one time level to the next by time splitting the evolution operator. First particles move freely across the domain without colliding, according to the equation:

$$\frac{\partial F}{\partial t} + \boldsymbol{\xi} \circ \nabla F = 0. \tag{26}$$

Then, the collisional step takes place and particle velocities are changed according to the equation:

$$\frac{\partial F}{\partial t} = J_E(F, F) \tag{27}$$

which *does not* describe a homogeneous relaxation, because of the non-local character of the collision integral in Eq. (2). Following the well known DSMC method (Bird, 1994) developed for the Boltzmann equation, at the particle level the collisional step is accomplished by using a majorant collision frequency scheme (Koura, 1986) to estimate the number of collisions which are going to occur in $\mathbb{D}$ within the time Δt. Particles are then selected in pairs and collide according to a collision probability derived from Eq. (1). Since the method is intrinsically designed to solve the unsteady Enskog equation, after preparing the particle system in a suitably chosen initial state, a number of time steps has to be computed until the transient dies out; then the sampling of the particle properties starts and the time averaged macroscopic quantities are obtained.

3.2. Test computations

Solutions have been obtained for various values of the flow parameters η_0, L, and T_2/T_1. The reference reduced density η_0 is computed from the flowfield average number density n_0 defined as:

$$n_0 = \frac{1}{L}\int_0^L n(x)dx. \tag{28}$$

A few cases have also been computed by other methods to increase confidence in the numerical results. In particular, the ideal gas limit ($\eta_0 \to 0$) offers the possibility of comparing the results of the present particle scheme with those obtained by a traditional DSMC method for the Boltzmann equation. Figure 1 shows a comparison of the profiles of density n, temperature T, stress tensor component P_{xx} and heat flux Q_x for the case $\eta_0 = 10^{-3}$, $L = 50\lambda_0$, $T_2/T_1 = 2$ with the corresponding profiles computed from the Boltzmann equation, solved by Koura's Null-Collision DSMC method (Koura, 1986). The density, temperature, stress and heat flux are normalized to $n_0, T_1, n_0 k T_1$ and $m n_0 (RT_1)^{3/2}$, respectively. The coordinate x and L are normalized to the reference mean free path $\lambda_0 = [\sqrt{2}\pi n_0 a^2 Y(n_0)]^{-1}$. The same particle number ($N_p = 50000$) and spatial grid layout (500 cells) have been used in both computations, which show very good agreement.

A direct discretization method (DDM) has been used to produce a few test computations in the case of a dense gas. In this method no particles are used; both the physical and velocity space have a finite size and they are divided into a number of cells in which the distribution function is assumed to be constant. A finite difference scheme is used to update the values of F in the free flight step described by Eq. (26), whereas a Monte Carlo quadrature technique is adopted to evaluate the collision integral in each cell and perform the collisional step,

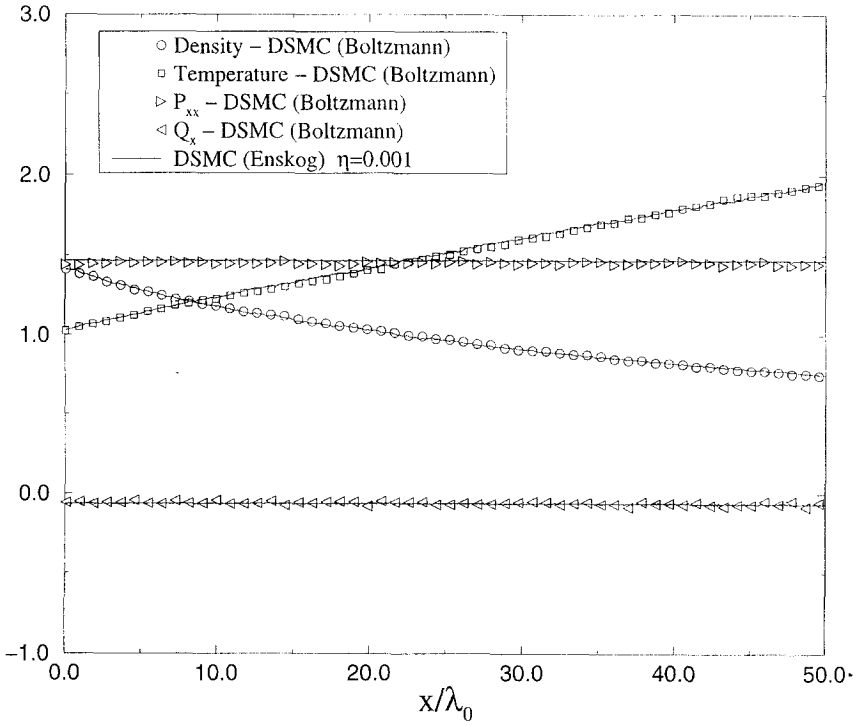

Fig. 1. – Comparison of a DSMC Boltzmann simulation with a DSMC solution of the Enskog equation for a dilute gas ($\eta_0 = 0.001$).

according to Eq. (27). DDM, described in detail by Frezzotti and Sgarra (1993), is the natural extension of a similar method developed by several authors (Nordsieck and Hicks, 1967; Aristov and Tcheremissine, 1980) to compute numerical solutions of the Boltzmann equation. Although DDM is capable of producing accurate and smooth solutions, it is more demanding than particle schemes in terms of computer memory and CPU time. As shown in figures 7, 8, where results obtained from DSMC and DDM are compared, there is very good agreement between the two methods. In the case to which figures 7, 8 refer, the reference reduced density η_0 is set to 0.2, L is set to $20\lambda_0$ and T_2/T_1 is equal to 2. The average density is typical of a gas held at room temperature and at a pressure of several hundred atmospheres, the mean free path λ_0 being only one third of the molecular diameter a. When compared to the dilute gas case, some of the profiles in figures 7, 8 exhibit not only quantitative but also qualitative differences. The density is no longer a monotonic decreasing function of x, but it oscillates close to the cold wall. These oscillatory density variations occur over a scale of the order of a. The number and the height of the peaks increase as the gas gets denser and denser (Snook and Henderson, 1978). The higher density values in the vicinity of the boundaries can be explained taking into account that, when the distance of a molecule from the wall is less than a, then a portion of its surface is protected from collisions, since there is no room left for a collision partner. The molecule is therefore pushed against the wall. Its is worth observing that this mechanism can produce values of the *local* density well above the close packing density ($\eta_{cp} \approx 0.742$), thus providing a good test for the approximate pair correlation function given by Eq. (11). The temperature curve is very close to a straight line and shows the characteristic "slip" effect at the boundaries (Cercignani, 1990). The potential contributions to P_{xx} and Q_x are now of the same order of magnitude as the kinetic parts. As shown in figures 7, 8, the sum of the kinetic and potential parts gives fairly constant P_{xx} and Q_x profiles. It is also worth noticing that the potential contributions $P_{xx}^{\rm pot}$ and $Q_x^{\rm pot}$ do vanish at the boundaries as required by Eqs. (19, 20). The number of particles in the DSMC computer simulations has been varied until little or no

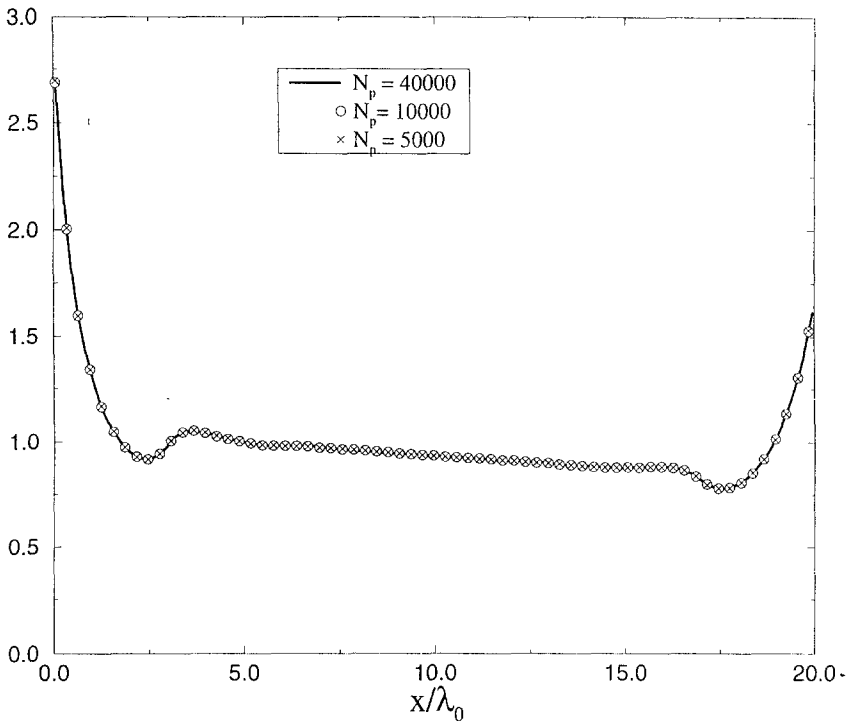

Fig. 2. – Effect of particle number on DSMC density profile. $L = 20\lambda_0, \eta_0 = 0.2, T_2/T_1 = 2$. Continuous line: $N_p = 40000$; ○ $N_p = 10000$; × $N_p = 5000$.

change is observed in the results. As shown in figure 2, very little change is produced by changing N_p from 5000 to 40000 if the number of time steps is tuned to have the same sample size at each spatial location.

3.3. Comparaison with MD simulation

The degree of approximation involved in Enskog's kinetic description of the hard sphere fluid can be checked through deterministic molecular dynamics (MD) simulations, in which the motion of a number of hard spheres is computed exactly from Newton's laws, probabilistic methods being usually confined to the choice of initial conditions only. Of course MD simulations are also affected by approximations which come from computers' finite arithmetic and from the constraints imposed on the number of simulation molecules by the computer memory and CPU time.

In the MD simulation of the heat conduction problem considered here, the infinite domain occupied by the gas has been replaced by a finite parallelepiped containing a relatively small number (from 1000 to 10000) hard spheres. The parallelepiped has been obtained by slicing the flowfield along the x direction. Accordingly, two of its faces are parallel to the walls and located at $x = 0$ and $x = L$, respectively. The parallelepiped's dimensions along the y and z directions have been adjusted to obtain the desired number of molecules in the flowfield. In complete analogy with the DSMC simulations, it has been assumed that a molecule hitting a wall is absorbed and immediately reemitted following boundary conditions (4,5). Periodic boundary conditions have been used at the parallelepiped faces normal to y and z directions. The minimum image convention (Allen and Tildesley, 1987) has usually been used for selecting collision partners, but the search has been extended to more distant images in the low density simulations. A series of parallel DSMC and MD simulations has been performed, in which the plate separation L and the temperature ratio T_2/T_1 has been kept fixed and the reference reduced

density η_0 has been gradually increased from 0.05 to 0.2. Furthermore, for each value of L and η_0, the density distribution between the plates has been changed by varying the plate temperature ratio. In fact, higher densities in front of the cold plate are produced by increasing T_2/T_1.

The results for the case $L = 20\lambda_0$, $\eta_0 = 0.05$ and $T_2/T_1 = 2$ are summarized in figures 3, 4. The density and temperature profiles, shown in figure 3, are in excellent agreement. The P_{xx}, $P_{xx}^{\rm pot}$ and $P_{xx}^{\rm kin}$ curves computed by the DSMC solution of the Enskog equation are also in very good agreement with the MD simulation (see Figure 3). The heat flux results, displayed in figure 4, are somewhat noisier, but both Q_x data sets are very well fitted by a horizontal straight line and their mean values are very close as shown in figure 12. The situation does not change appreciably when the reduced density is raised to 0.1 (see Figures 5, 6), but, as shown in figure 7, when the value $\eta_0 = 0.2$ is reached, some discrepancies appear, mainly in the density profile in the region where oscillations occur. It is possible to observe that the density peaks of the MD simulation are more pronounced. The maximum deviation of the DSMC density profile from MD results amounts to about 9%, but it does not lead to similar discrepancies in the temperatures. The P_{xx} and Q_x profiles, shown in figures 7, 8 remain rather close, too. The mean values of P_{xx} and Q_x computed by MD are slightly above the DSMC results which lay within one standard deviation, anyway. As expected, larger discrepancies are found when higher density values are obtained in the vicinity of the cold wall, by raising T_2/T_1 to 4. Two cases have been computed with the above temperature ratio: the first with $L = 20\lambda_0$ and the second with the larger plate separation $L = 50\lambda_0$ which causes an even higher density peak. As shown in figures 9 and 11, the maximum deviation of the density profile predicted by Enskog equation amounts to 13% of the MD results in the first case and to 20% in the second one. As in the previous examples, the discrepancy is limited to the oscillatory region. It is possible to observe that now the DSMC temperature profiles also deviate from MD in the low temperature region of the flowfield. Small deviations of the DSMC results from MD's are also observed for P_{xx} and Q_x profiles shown

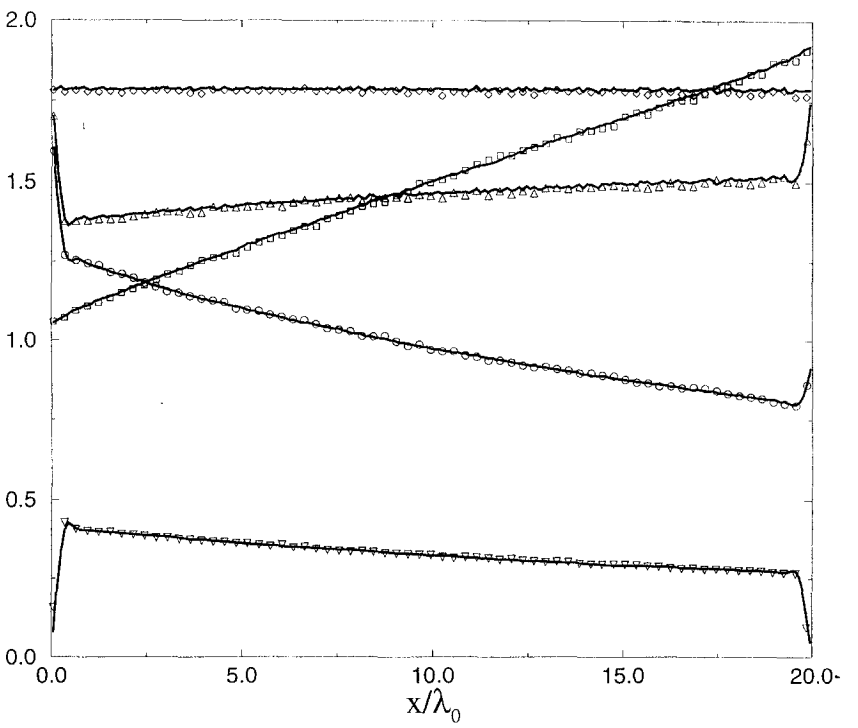

Fig. 3. – Comparison of DSMC and MD results. $L = 20\lambda_0, \eta_0 = 0.05, T_2/T_1 = 2$. Continuous lines: DSMC; ○ MD normalized density; □ MD normalized temperature; ◇ MD P_{xx}; ▽ MD $P_{xx}^{\rm pot}$; △ MD $P_{xx}^{\rm kin}$.

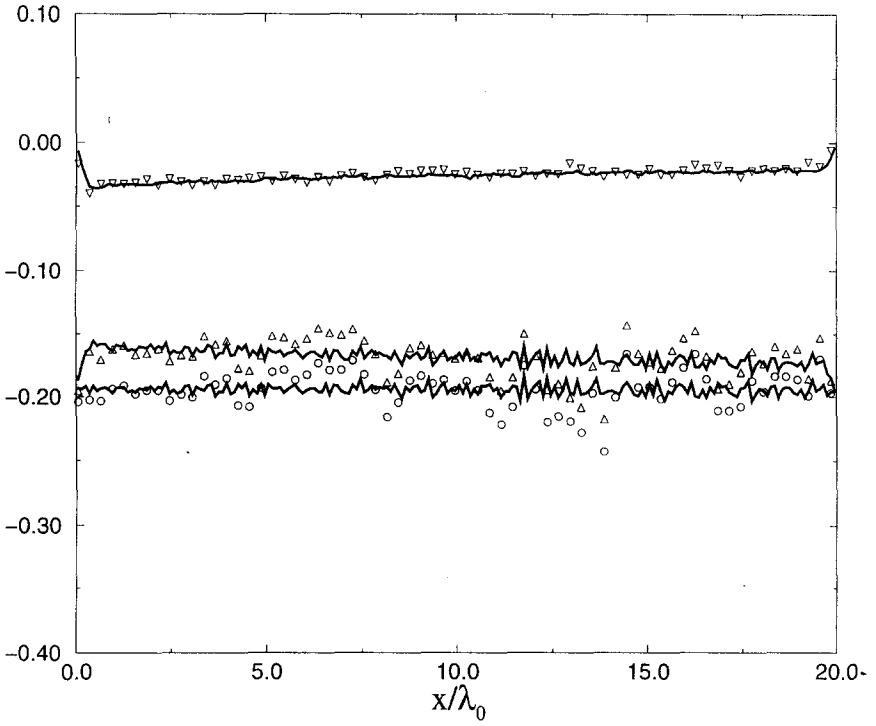

Fig. 4. – Comparison of DSMC and MD results. $L = 20\lambda_0$, $\eta_0 = 0.05$, $T_2/T_1 = 2$. Continuous lines: DSMC; ○ MD Q_x; ▽ MD $Q_x^{\rm pot}$; △ MD $Q_x^{\rm kin}$.

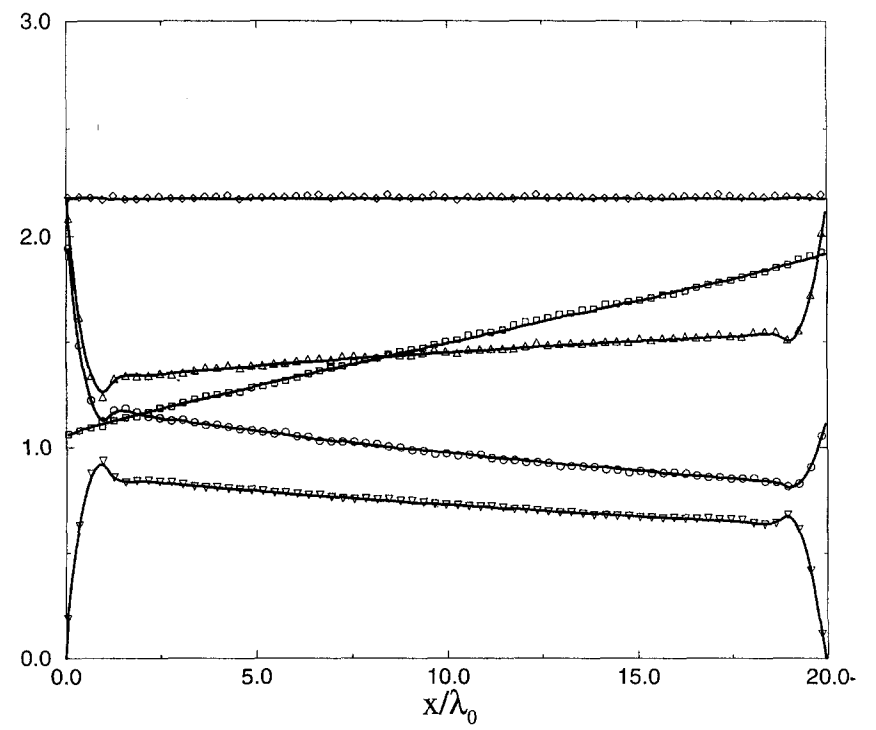

Fig. 5. – Comparison of DSMC and MD results. $L = 20\lambda_0$, $\eta_0 = 0.1$, $T_2/T_1 = 2$. Continuous lines: DSMC; ○ MD normalized density; □ MD normalized temperature; ◇ MD P_{xx}; ▽ MD $P_{xx}^{\rm pot}$; △ MD $P_{xx}^{\rm kin}$.

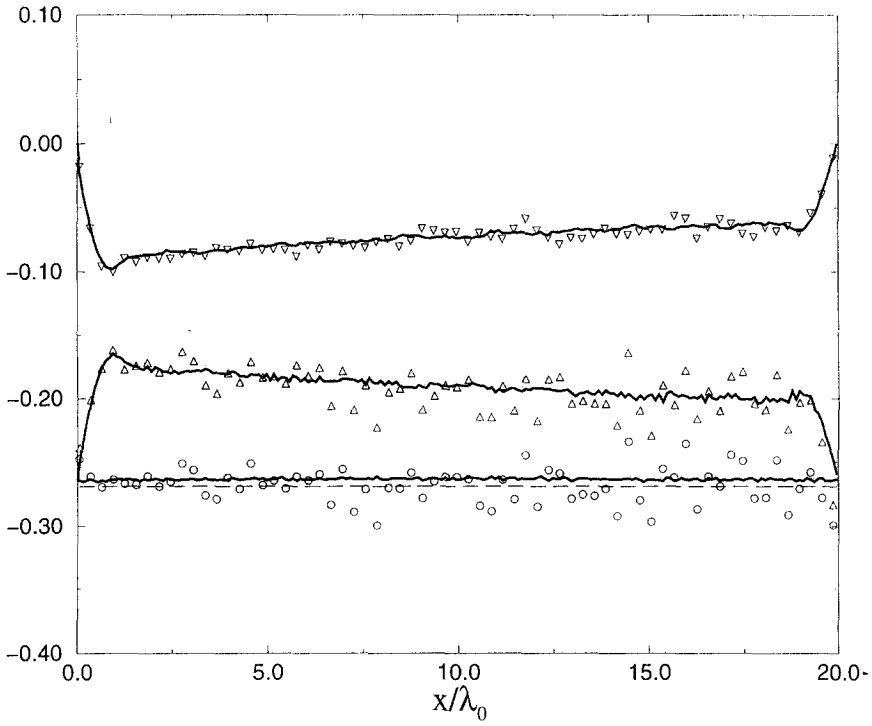

Fig. 6. – Comparison of DSMC and MD results. $L = 20\lambda_0$, $\eta_0 = 0.1$, $T_2/T_1 = 2$. Continuous lines: DSMC; ○ MD Q_x; ▽ MD $Q_x^{\rm pot}$; △ MD $Q_x^{\rm kin}$; dashed line: Q_x, best fit of MD data.

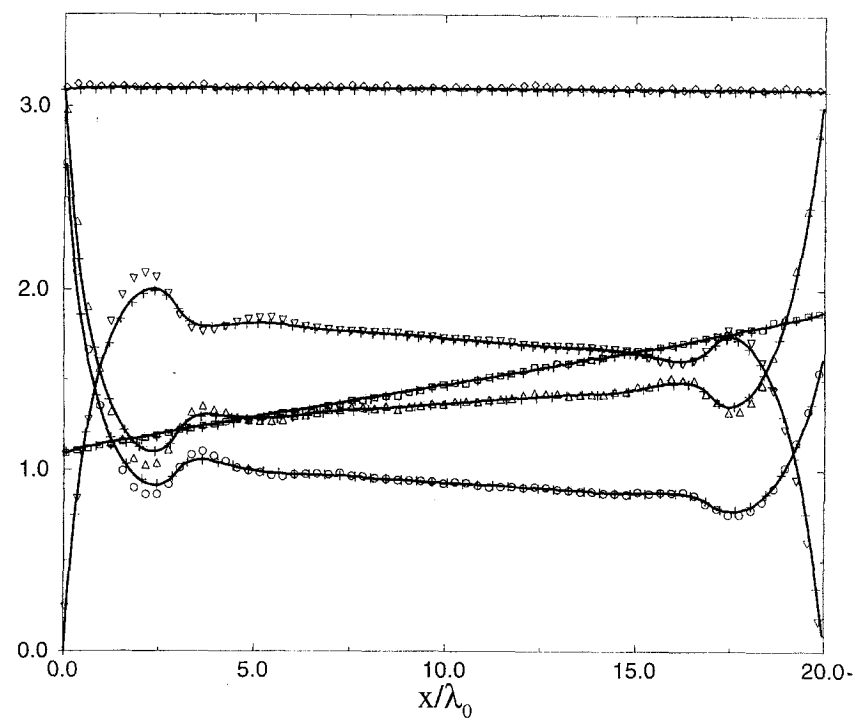

Fig. 7. – Comparison of DSMC, DDM and MD results. $L = 20\lambda_0$, $\eta_0 = 0.2$, $T_2/T_1 = 2$. Continuous lines: DSMC; × DDM; ○ MD normalized density; □ MD normalized temperature; ◇ MD P_{xx}; ▽ MD $P_{xx}^{\rm pot}$; △ MD $P_{xx}^{\rm kin}$.

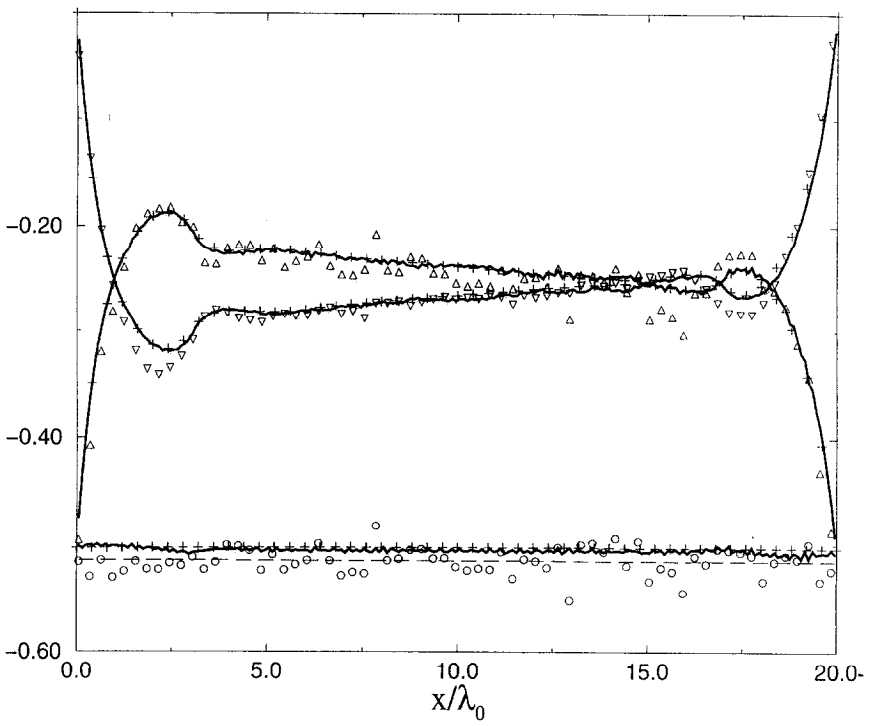

Fig. 8. – Comparison of DSMC, DDM and MD resultts. $L = 20\lambda_0$, $\eta_0 = 0.2, T_2/T_1 = 2$. Continuous lines: DSMC; × DDM; ○ MD Q_x; ▽ DDM $Q_x^{\rm pot}$; △ MD $Q_x^{\rm kin}$; dashed line: Q_x, best fit of MD data.

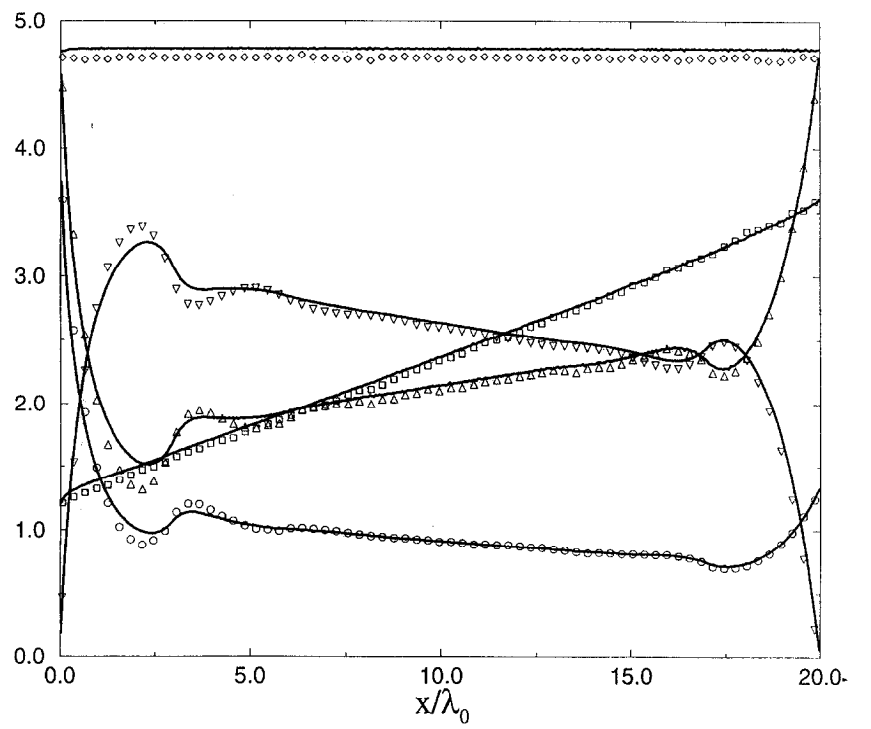

Fig. 9. – Comparison of DSMC and MD results. $L = 20\lambda_0$, $\eta_0 = 0.2$, $T_2/T_1 = 4$. Continuous lines: DSMC; ○ MD normalized density; □ MD normalized temperature; ◇ MD P_{xx}; ▽ MD $P_{xx}^{\rm pot}$; △ MD $P_{xx}^{\rm kin}$.

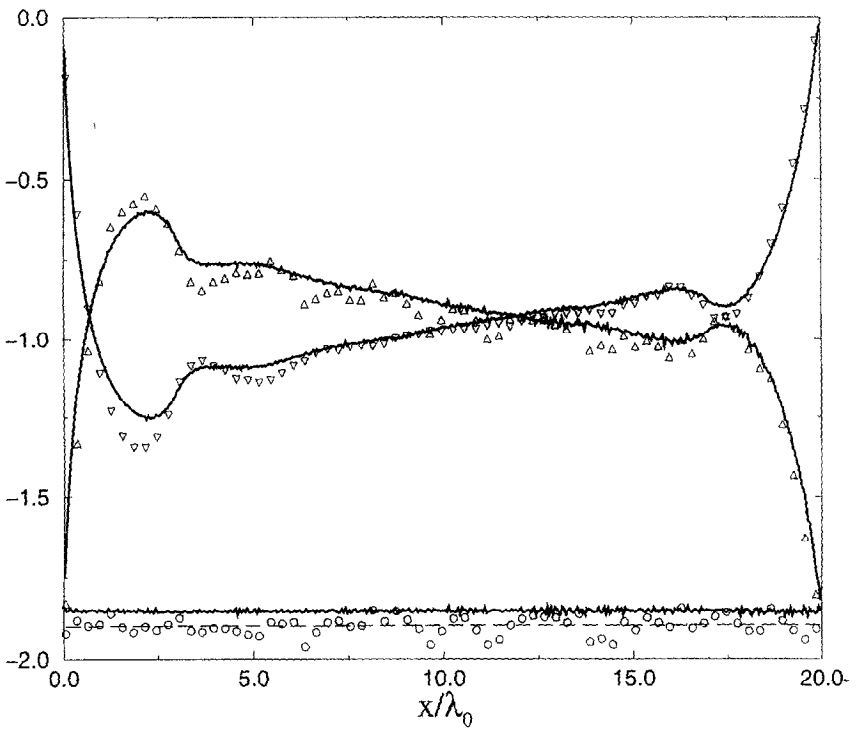

Fig. 10. – Comparison of DSMC and MD results. $L = 20\lambda_0$, $\eta_0 = 0.2$, $T_2/T_1 = 4$. Continuous lines: DSMC; ○ MD Q_x; ▽ MD $Q_x^{\rm pot}$; △ MD $Q_x^{\rm kin}$; dashed line: Q_x, best fit of MD data.

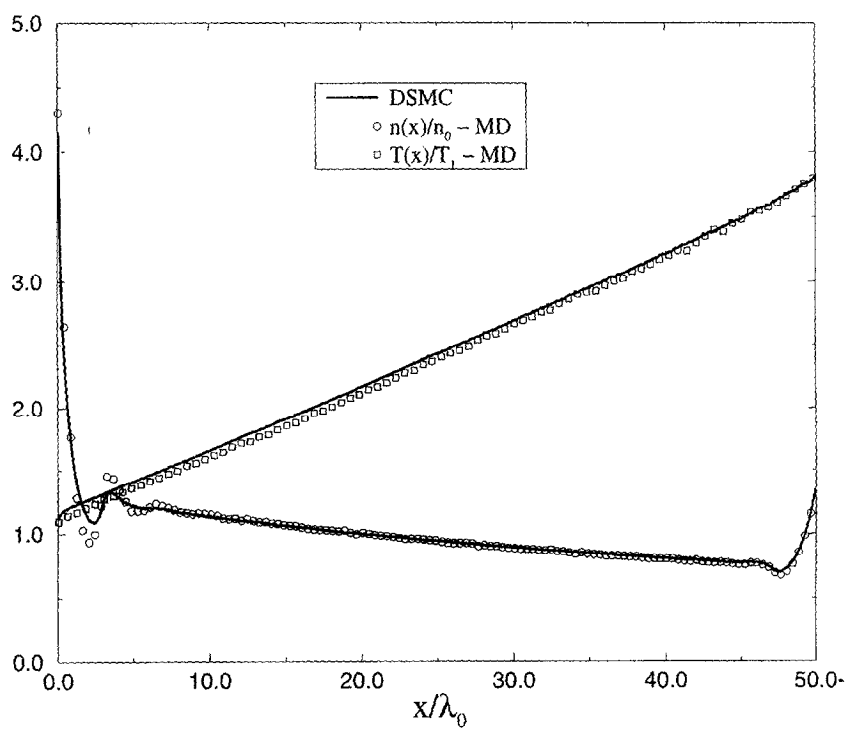

Fig. 11. – Comparison of DSMC and MD results. $L = 50\lambda_0$, $\eta_0 = 0.2$, $T_2/T_1 = 4$. Continuous lines: DSMC; ○ MD normalized density; □ MD normalized temperature.

in figures 9, 10. Discrepancies amount to about 2% for the total P_{xx} and Q_x, but larger deviations are found for the potential and kinetic contributions, particularly in the region where the density error is also larger. However, the deviations have opposite signs and partially compensate to give a smaller error on the total values. It is interesting to note that in all the cases with $\eta_0 = 0.2$, the local reduced density $\eta(x)$ exceeds the limiting value 0.47 close to the cold wall. In the last case examined ($L = 50\lambda_0, \eta_0 = 0.2, T_2/T_1 = 4$), the highest η is even well above the close packing reduced density η_{cp}. This last example is also very close to the computational limit imposed by the singularity of $Y(n)$ in $\eta = 1$. In fact, when higher values of η_0 or T_2/T_1 are considered, the density fluctuations may bring $\eta(x)$ very close to 1. In this case the collision rate becomes very high and the time step has to be reduced to such a small value as to make the computation absolutely impractical.

3.4. Comparison with continuum theory

The heat conduction problem considered in this paper can also be approached by continuum theory which leads to a much simpler mathematical formulation:

$$-\chi(n,T)\frac{dT}{dx} = Q_x = const. \tag{29}$$

$$p = p(n,T) = const. \tag{30}$$

In Eq. (29) $\chi(n,T)$ is the gas thermal conductivity, whereas $p(n,T)$ is the equation of state specified by Eq. (9). The expression for $\chi(n,T)$ can be obtained by the Chapman-Enskog expansion associated to Eq. (1) as shown in Chapman and Cowling (1960) and Resibois and DeLeener (1977). The constant values of Q_x and p are fixed by the conditions:

$$T(0) = T_1 \tag{31}$$

$$T(L) = T_2 \tag{32}$$

$$\frac{1}{L}\int_0^L n(x)dx = n_0 \tag{33}$$

Numerical solution of the differential equation (29) can be easily computed by a finite difference scheme. The values of the heat flux computed from continuum theory are compared to DSMC and MD results in figures 12 ($T_2/T_1 = 2$) and 13 ($T_2/T_1 = 4$). As expected, continuum theory considerably overestimates the correct heat flux for the smallest values of the wall separation, where nonequilibrium effects are stronger, the discrepancy being more pronounced for denser fluids. For $L = 50\lambda_0$ the agreement between continuum and kinetic theory is better, particularly for the moderately dense fluids. Examples of continuum theory spatial profiles are given in figures 14, 15. In the first case the reference reduced density is 0.2, the plate separation is $L = 20\lambda_0$ and T_2/T_1 is 4. Besides the already mentioned discrepancy in Q_x, it is possible to observe the difference between the pressure p and the DSMC P_{xx} value. The temperature profiles are qualitatively similar, but, of course, there is no temperature "slip" in the continuum profile; the continuum density profile is monotonic since the prediction of the oscillatory behaviour is beyond the capabilities of such a simple approach. In the second example the wall separation is larger ($L = 50\lambda_0$) and the previous value of the temperature ratio and reduced density are

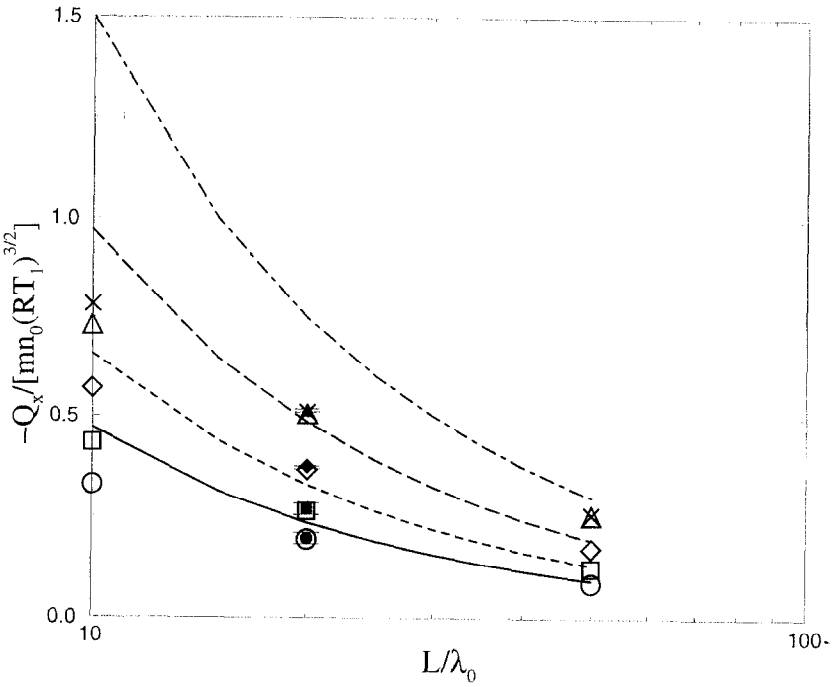

Fig. 12. – Total heat flux vs. plates-separation. $T_2/T_1 = 2$. Lines: continuum theory. Continuous line $\eta_0 = 0.05$; dashed line $\eta_0 = 0.1$; long dashed line $\eta_0 = 0.15$; dashed-dotted line $\eta_0 = 0.2$. ○ DSMC $\eta_0 = 0.05$; □ DSMC $\eta_0 = 1$; ◇ DSMC $\eta_0 = 0.15$; △ DSMC $\eta_0 = 0.2$. Filled symbols: MD results. × Averaged Q_x computed from DSMC density and temperature profiles and Fourier law [Eq. (29)].

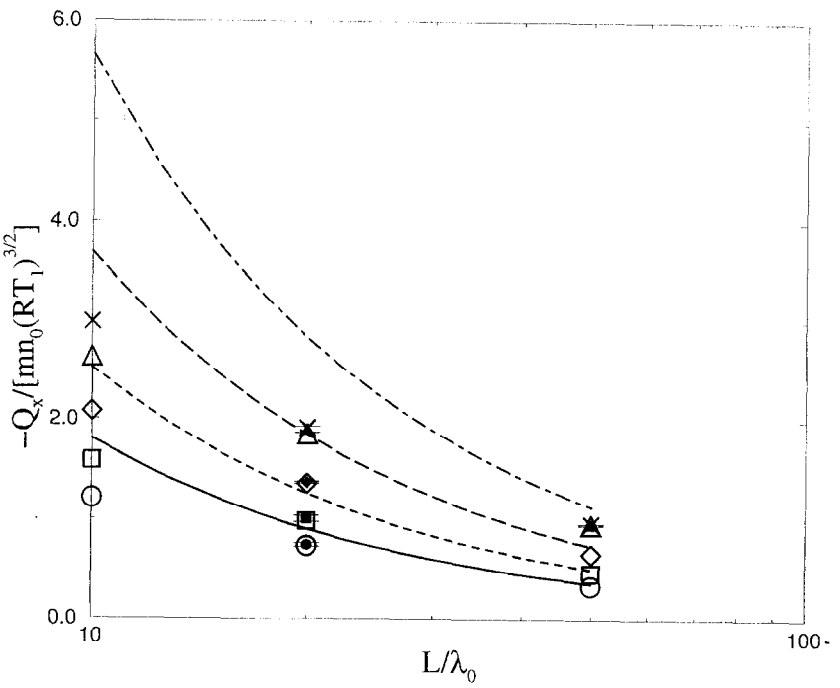

Fig. 13. – Total heat flux vs. plates separation. $T_2/T_1 = 4$. Lines: continuum theory. Continuous line $\eta_0 = 0.05$; dahsed line $\eta_0 = 0.1$; long dashed line $\eta_0 = 0.15$; dashed-dotted line $\eta_0 = 0.2$. ○ DSMC $\eta_0 = 0.05$; □ DSMC $\eta_0 = 0.1$; ◇ DSMC $\eta_0 = 0.15$; △ DSMC $\eta_0 = 0.2$. Filled symbols MD results. × Averaged Q_x computed from DSMC density and temperature profiles and Fourier law [Eq. (29)].

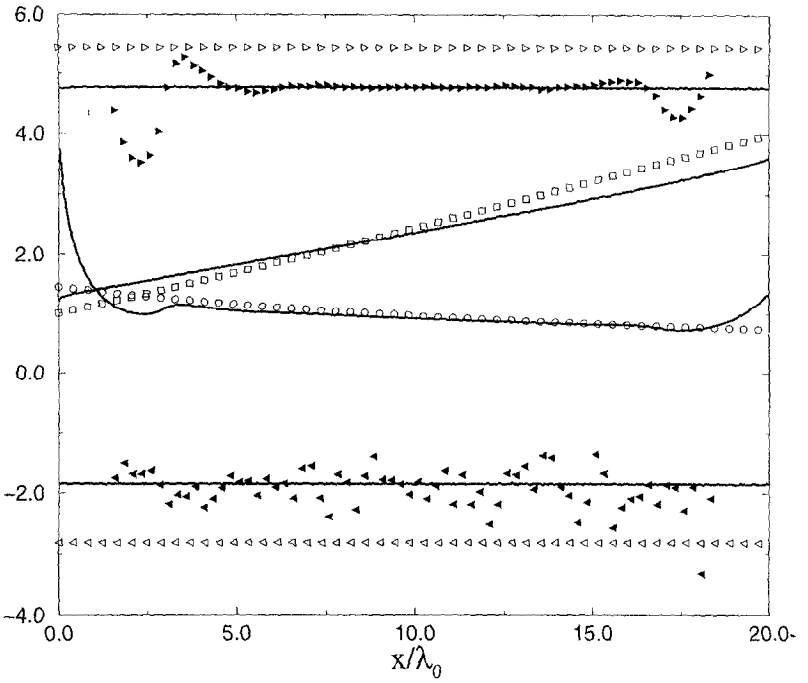

Fig. 14. – Comparison of continuum theory and DSMC profiles. $L = 20\lambda_0$, $\eta_0 = 0.2$, $T_2/T_1 = 4$. Continuous lines DSMC; ○ continuum theory density; □ continuum theory temperature; ▷ continuum theory p; ◁ continuum theory Q_x; filled ▷ p computed from equation of state [Eq. (30)] and DSMC density and temperature data; filled ◁ Q_x computed from Fourier law [Eq. (29)] and DSMC density and temperature data.

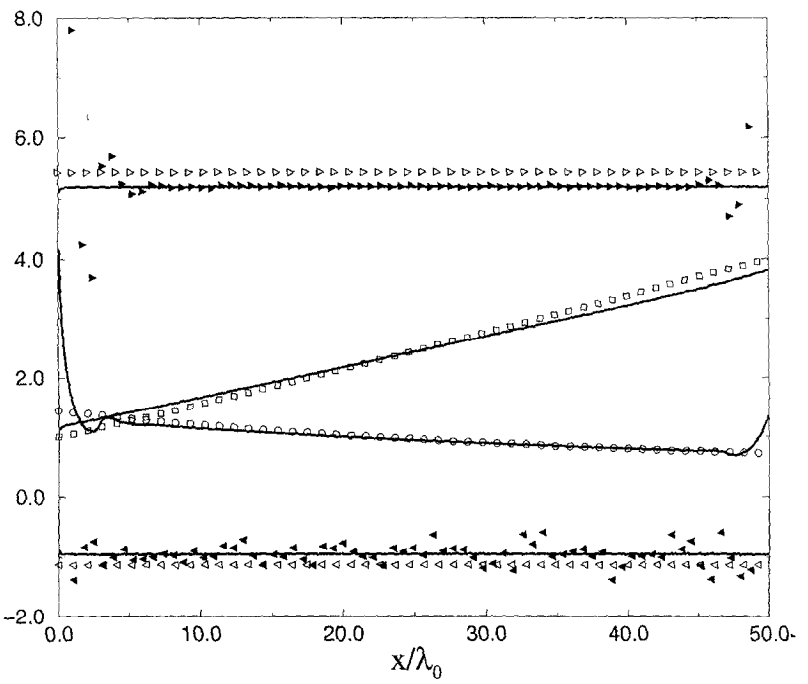

Fig. 15. – Comparison of continuum theory and DSMC profiles. $L = 50\lambda_0$, $\eta_0 = 0.2$, $T_2/T_1 = 4$. Continuous lines DSMC; ○ continuum theory density; □ continuum theory temperature; ▷ continuum theory p; ◁ continuum theory Q_x; filled ▷ p computed from equation of state [Eq. (30)] and DSMC density and temperature data; filled ◁ Q_x computed from Fourier law [Eq. (29)] and DSMC density and temperature data.

kept. Now the results of continuum theory are better: the heat flux value is closer to the DSMC prediction, the temperature profiles are also closer, since the temperature jumps of the kinetic theory solution are smaller. The continuum density profile also agrees very well with the DSMC simulation in most points of the flowfield, the discrepancies being confined to a narrow region close to the walls.

It should be pointed out that the discrepancies between continuum and kinetic theory can be mainly attributed to the use of non-slip boundary conditions rather than to a deficiency of Fourier law. If, following Montanero et al. (1994), DSMC density and temperature profiles are inserted into Eqs. (29, 30), it is possible to observe (see Figures 13, 14) that the computed values of pressure p and heat flux Q_x turn out to be very close to kinetic theory results in the central part of the flowfield, where the effects of boundaries are smaller.

4. Conclusions

As already stated in the introduction, the aim of this paper is the assessment of the capability of Eq. (1) in the study of the hard sphere fluid in nonequilibrium conditions. The problem considered, the steady heat flow between parallel plates, has been chosen for its geometrical simplicity which makes the use of different numerical techniques possible. A secondary aim of the work is the testing of the DSMC-like particle scheme used to compute the numerical solutions of the Enskog equation. As shown in section 3.2, good agreement has been found with a traditional DSMC Boltzmann scheme in the ideal gas limit, and, in the dense gas case, with a method based on a finite difference discretization of Eq. (1) combined with Monte Carlo quadrature.

The ability of Eq. (1) to reproduce the correct behaviour of a hard sphere gas has been tested against deterministic molecular dynamics simulations. Starting from a moderately dense fluid, solutions with increasing values of the reference reduced density have been obtained. The results show that the agreement between the numerical solutions of Eq. (1) and the MD results is very good as long as the local reduced density remains within the validity range of the Carnahan-Starling equation of state, from which the approximated pair correlation function has been obtained. As discussed in section 3.3, when the gas density increases, the local reduced density considerably exceeds the limits imposed by Eq. (9) at some flowfield points. Therefore it is not surprising that the various approximations involved in Eq. (1) do manifest themselves by producing incorrect results. However it should be observed that, even when η is above the packing density, the deviations of the DSMC results from MD's are practically limited to the oscillatory part of the density profiles. The temperature profile is rather well reproduced as well as the values of the heat flux summarized in figures 19, 20.

For the problem considered here, the deviation of DSMC solutions from MD results at high density is likely to be related to the use of the uniform equilibrium pair correlation function in Eq. (1), rather than to a failure of the Carnahan-Starling approximation. In fact, the Y function given by Eq. (11) can be replaced by an expression (Sanchez, 1994) which is more accurate in the vicinity of the close packing density. However, some preliminary computations show little or no change with respect to the results presented here.

Finally, it is worth mentioning that a more refined approach to the kinetic theory of the hard sphere gas is provided by the modified Enskog equation (van Beijeren and Ernst, 1973), in which the *uniform equilibrium* pair correlation function is replaced by the *local equilibrium* pair correlation function. The modified equation is unfortunately much more complicated than Eq. (1), since a function of the density is replaced by a functional of the density whose computation is far from being trivial. However, it has better theoretical properties. For instance, it gives the exact solution for a gas in equilibrium in an external force field, whereas Eq. (1) does not (van Beijeren, 1983). It is therefore quite possible that the modified Enskog equation may perform better than Eq. (1) in the problem considered here.

Acknowledgement. – The author wishes to thank one of the referees for bringing Montanero et al. (1994) and Sanchez (1994) to his attention.

REFERENCES

ALLEN M. P., TILDESLEY D. J., 1987, *Computer Simulation of Liquids,* Clarendon Press, Oxford.

ARISTOV V. V., TCHEREMISSINE F. G., 1980, The Conservative Splitting Method for Solving the Boltzmann Equation, *USSR Comp. Math. Phys.,* **20**, 208.

BALESCU R., 1975, *Equilibrium and Nonequilibrium Statistical Mechanics,* John Wiley & Sons, New York.

BIRD G. A., 1994, *Molecular Gas Dynamics and the Direct Simulation of Gas Flows,* Clarendon Press, Oxford.

CARNAHAN N. F., STARLING K. E., 1969, Equation of State for Nonattracting rigid spheres, *J. Chem. Phys.,* **51**, 635.

CERCIGNANI C., 1990, *Mathematical Methods in Kinetic Theory,* Plenum Press, New York.

CERCIGNANI C., LAMPIS M., 1988, On the Kinetic Theory of a Dense Gas of Rough Spheres, *Journal of Statistical Physics,* **53** (3/4), 655–672.

CHAPMAN S., COWLING T. G., 1960, *The Mathematical Theory of Nonuniform Gases,* Cambridge University Press, Cambridge.

ENSKOG D., 1922, Kinetische Theorie der Waerme Leitung, Reibung und Selbstdiffusion in Gewissen Verdichten Gasen und Fluessigkeiten. *Kungl. Svenska Veteenskapakad. Handl.,* **63**, 3–44.

FREZZOTTI A., 1997a, Molecular Dynamics and Enskog Theory Calculation of One Dimensional Problems in the Dynamics of Dense Gases, *Physica A,* **240**, 202–211.

FREZZOTTI A., 1997b, A Particle Scheme for the Numerical Solution of the Enskog Equation, *Physics of Fluids,* **9** (5), 1329–1335.

FREZZOTTI A., 1998, Molecular Dynamics and Enskog Theory Calculation of Shock Profiles in a Dense Hard Sphere Gas, *Computers Math. Applic.,* **35** (1/2), 103–112.

FREZZOTTI A., SGARRA C., 1993, Numerical Analysis of a Shock Wave Solution of the Enskog Equation Obtained via a Monte Carlo Method, *J. Stat. Phys.,* **73**, 193–207.

KOURA K., 1986, Null-Collision Technique in the Direct Simulation Monte Carlo Method, *Phys. Fluids A,* **29**, 3509–3511.

MONTANERO J., ALAUI M., SANTOS A., GARZÓ V., 1994, Monte Carlo simulation of the Boltzmann equation for steady Fourier flow, *Phys. Rev. E,* **49** (1), 367–375.

NORDSIECK A., HICKS B., 1967, Monte Carlo Evaluation of the Boltzmann Collision Integral. In *Rarefied Gas Dynamics,* edited by C. L. BRUNDIN, Vol. 2, New York, Academic Press.

RESIBOIS P., DELEENER M., 1977, *Classical Kinetic Theory of Fluids,* J. Wiley & Sons, New York.

SANCHEZ I. C., 1994, Virial coefficients and close packing of hard spheres and disks, *J. Chem. Phys.,* **101** (8), 7003–7006.

SNOOK I. K., HENDERSON D., 1978, Monte Carlo Study of a Hard-Sphere Fluid near a Hard Wall, *J. Chem. Phys.,* **68** (5), 2134–2139.

VAN BEIJEREN H., 1983, Equilibrium Distribution os Hard-sphere System and Revised Enskog Theory, *Physical Review Letters,* **51**, 1503–1505.

VAN BEIJEREN H., ERNST M. H., 1973, The Modified Enskog Equation, *Physica,* **68**, 437–456.

(Received 11 November 1997;
revised and accepted 3 March 1998.)